

# Multiple plasmon resonances in naturally-occurring multiwall nanotubes: infrared spectra of chrysotile asbestos

Etienne Balan<sup>1</sup>, Francesco Mauri<sup>1</sup>, Celine Lemaire<sup>1</sup>, Christian Brouder<sup>1</sup>, Francois Guyot<sup>1</sup>, A. Marco Saitta<sup>2</sup>, and Bertrand Devouard<sup>3</sup>

<sup>1</sup>Laboratoire de Minéralogie Cristallographie, case 115, 4 place Jussieu, 75252 Paris cedex 05, France

<sup>2</sup>Laboratoire de Physique des Milieux Condensés, 4 Place Jussieu, 75252 Paris cedex 05, France

<sup>3</sup>Laboratoire Magmas et Volcans, 5 rue Kessler, 63038 Clermont-Ferrand cedex, France

(Dated: April 14, 2024)

Chrysotile asbestos is formed by densely packed bundles of multiwall hollow nanotubes. Each wall in the nanotubes is a cylindrically wrapped layer of  $Mg_3Si_2O_5(OH)_4$ . We show by experiment and theory that the infrared spectrum of chrysotile presents multiple plasmon resonances in the Si-O stretching bands. These collective charge excitations are universal features of the nanotubes that are obtained by cylindrically wrapping an anisotropic material. The multiple plasmons can be observed if the width of the resonances is sufficiently small as in chrysotile.

PACS numbers: 78.67.Ch, 63.22.+m, 73.20.Mf, 91.60.-x

The interaction of nanostructures with electromagnetic waves has recently received an increasing attention, both because of fundamental and technological issues. The frequency dependence of this interaction is governed by different phenomena according to the characteristic size of the nanostructure template. The regime dominated by interference and diffraction occurs for particle sizes close to the wavelength of light as, e.g., in photonic crystals or in opals. The regime dominated by quantum mechanics occurs for sizes close to or smaller than a few nanometers such as in quantum dots or nanocrystals. Between these two regimes, a third regime occurs where the frequency dependence is dictated by collective charge excitations, i.e. by confined plasmons [1, 2, 3, 4, 5, 6]. In this regime, an interesting phenomenon occurs in multiwall nanotubes that are obtained by wrapping around cylinders layers of an anisotropic material, as in carbon [1, 4, 5] or  $WS_2$  [6] nanotubes. In particular, the macroscopic dielectric tensor,  $\epsilon^\omega(\mathbf{k})$ , of the nanotubes can present multiple confined plasmon resonances, that correspond to a single resonance in the dielectric tensor of the same material with flat planar layers. Such phenomenon has been observed in theoretical calculations [5]. Experimental measurements exist in the energy range of electronic excitations ( $\hbar\omega \sim 5-25$  eV) [2, 4, 5, 6]. However, in these experiments, the multipoint spectrum exhibits only one broad resonance because of the large width of the electronic resonances of the corresponding planar materials [5].

By contrast, the resonances of  $\epsilon^\omega(\mathbf{k})$  related to the ionic vibrations, in the infrared (IR) range ( $\hbar\omega \sim 0.1$  eV), are ideal candidates for the detection of multipoint spectra produced by collective charge excitations. In fact, the ionic resonances are much sharper than those related to the electronic excitations. Thus, in ionic materials with intense IR activity, multiple plasmons could be expected. Here, we show that the IR spectra of chrysotile asbestos present, indeed, multiple plasmon peaks related to its

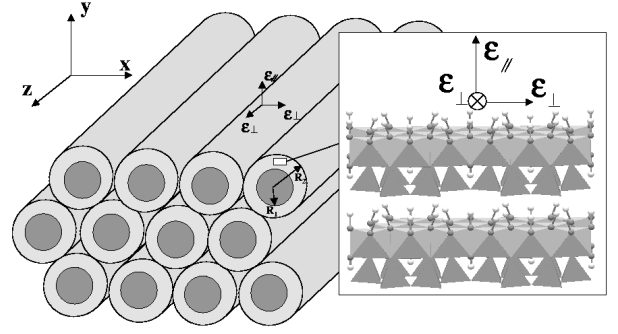


FIG. 1: Multiwall nanotubes of chrysotile, arranged as a hexagonal close packed array. The cylinders are infinitely long in the  $z$  direction. Inset: Structure of lizardite showing the stacking of two layers.

peculiar tubular nanostructure.

Chrysotile asbestos is an example of natural multiwall hollow nanotubes with  $Mg_3Si_2O_5(OH)_4$  composition, belonging to the group of serpentine minerals. These minerals are formed by stacking layers, each containing a pseudo-hexagonal silica sheet of corner-shared  $SiO_4$  units linked to a trioctahedral sheet of edge sharing  $MgO_2(OH)_4$  octahedra (Fig. 1). The OH groups located at the top of the trioctahedral sheet are H-bonded with the O of the basal plane of the next layer. These minerals present cylindrically wrapped layers in chrysotile, corrugated layers in antigorite, and flat layers in lizardite [7, 8]. The structural relation between chrysotile and lizardite is the same as that between C nanotubes and graphite. Chrysotile nanotubes present outer and inner diameters of 240–600 Å and 50–100 Å, respectively (Fig. 2). The tubes are arranged as densely packed bundles of parallel fibers, forming veins up to several centimeters thick.

We measure the IR spectra, in transmission and attenuated total reflectance (ATR), of a chrysotile sample from the asbestos mines of Salt River Canyon, Arizona.

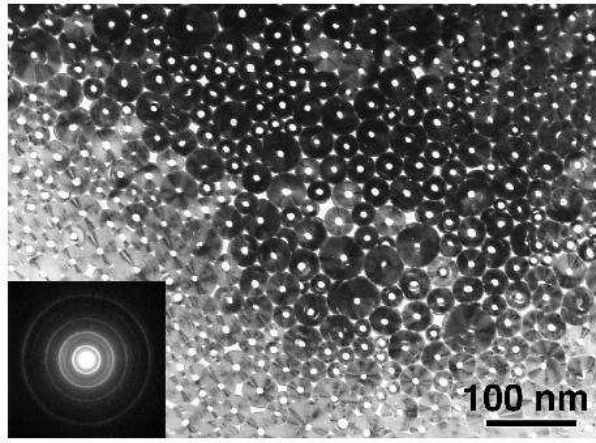


FIG. 2: Transmission electron microscopy of the investigated chrysotile sample, perpendicular to the tube axes. Inset: selected area electron diffraction pattern showing the parallel texture of chrysotile tubes seen along [100].

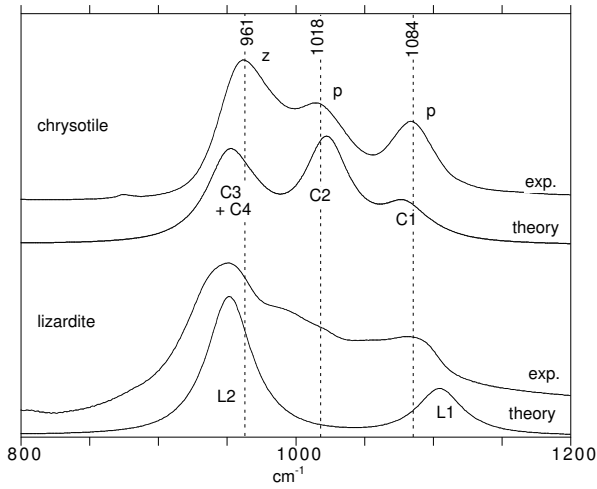


FIG. 3: Transmission powder IR absorption spectra of chrysotile and lizardite in KBr pellets (absorbance units). Spectra are recorded at room temperature using an FT-IR spectrometer Nicolet Magna 560 with a resolution of  $2 \text{ cm}^{-1}$ . z and p denote polarizations parallel and perpendicular to the tube axis, respectively.

zona. The sample, characterized by transmission electron microscopy and electron microprobe, consists of pure chrysotile tubes in parallel texture (Fig. 2). The IR powder spectrum of chrysotile, compared to that of the at-layered variety lizardite, displays a strong absorption band at  $1018 \text{ cm}^{-1}$  in the range of Si-O stretching vibrations (Fig. 3) (see also [9, 10, 11, 12]). The shoulder observed at  $1018 \text{ cm}^{-1}$  in the lizardite spectrum is indeed related to chrysotile and polygonal serpentine contaminations present in low amount in natural lizardite samples [11, 13]. In the IR powder spectrum of lizardite, the band at  $1084 \text{ cm}^{-1}$  ( $L_1$ , Tab. I) is related to the out-of-plane (perpendicular to the layers) Si-O stretching

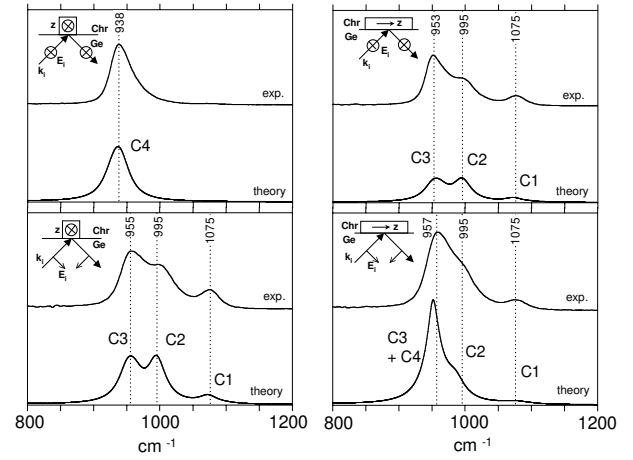


FIG. 4: Attenuated total reflectance IR spectra of chrysotile. Spectra in absorbance units are recorded with an ATR Thunderridge device equipped with an AgBr polarizer. The orientation of the chrysotile aggregate with respect to the incident IR wave is indicated; Chr: chrysotile; Ge: germanium crystal.

mode, whereas that at  $951 \text{ cm}^{-1}$  ( $L_2$ , Tab. I) is related to the two degenerate in-plane (parallel to the layers) Si-O stretching modes [13]. The bands at  $961$  and  $1018 \text{ cm}^{-1}$  of chrysotile were previously related to the lift of this degeneracy by the bending of the tetrahedral sheets [10]. We better constrain the dependence of the IR spectrum as a function of the polarization of the incident wave, by recording the ATR IR spectra of an oriented chrysotile aggregate. In this experiment, a thick oriented sample of chrysotile is pressed onto a Ge crystal. The spectrum of the IR light propagating in the Ge crystal and reflected at the chrysotile/Ge interface is recorded. The IR light has an incidence angle of  $45^\circ$ . The propagation and electric field vectors of the incident wave are set either parallel or perpendicular to the fiber axis and to the incidence plane, respectively (Fig. 4). The ATR spectrum recorded with the electric field vector parallel to the fiber axis displays only one band, whereas the three other spectra display three bands.

Since the size of the nanostructure template is much smaller than the wavelength of light, the IR spectrum is fully defined by the macroscopic dielectric tensor of chrysotile  $\epsilon_c(\omega)$ . To model the spectra, we consider, for simplicity, a nano-structured material composed of a close-packed array of mono-dispersed nanotubes (Fig. 1). An accurate effective medium theory has been derived for such systems [4]. However, here we compute  $\epsilon_c(\omega)$  from the polarisability of a single tube using a simple Clausius-Mossotti model, given the approximations made on the size distribution and on the arrangement of the tubes.

The polarisability  $\alpha(\omega)$  is calculated from the macroscopic dielectric tensor of the planar material, lizardite. The dielectric properties of an isolated tube in vacuum can be derived by assuming that the chrysotile tube is a dielectric continuum, locally identical to lizardite. Thus

the layer curvature is accounted for only at the macroscopic scale, as in Refs. [1, 4, 6]. The low-frequency dielectric tensor of lizardite,  $\epsilon_L(\omega)$ , can be written in Cartesian coordinates as:

$$\epsilon_L(\omega) = \epsilon_{xx}(\omega)u_xu_x + \epsilon_{yy}(\omega)u_yu_y + \epsilon_{zz}(\omega)u_zu_z; \quad (1)$$

where  $u_z$  corresponds to the  $c$  axis of the lizardite hexagonal structure, and  $\omega$  is the frequency of the IR wave. In Ref. [13], we have obtained the theoretical  $\epsilon_L(\omega)$  from the dynamical matrix and the effective charge tensors. These quantities were calculated from first-principles using density functional perturbation theory [14]. In the present study, we use  $\epsilon_L(\omega)$  of Ref. [13] calculated with a damping coefficient of  $16 \text{ cm}^{-1}$ . However, to better fit the experimental IR spectrum of lizardite, we shift the transverse optical frequency of the two degenerate in-plane Si-O stretching modes from the theoretical value of  $915 \text{ cm}^{-1}$  [13] to the experimental value of  $951 \text{ cm}^{-1}$ . The resulting theoretical IR powder spectrum of lizardite, obtained following [13, 15], is reported in Fig. 3.

The microscopic dielectric tensor of a chrysotile tube is

$$\epsilon_C(\omega; r; \omega) = \epsilon_{zz}(\omega)u_zu_z + \epsilon_{rr}(\omega)u_ru_r + \epsilon_{\theta\theta}(\omega)u_\theta u_\theta; \quad (2)$$

for  $R_1 < r < R_2$ , and  $\epsilon_C(\omega; r; \omega) = 1$  otherwise. Here  $u_z$ ,  $u_r$  and  $u_\theta$  are now the unitary basis vectors of cylindrical coordinates and  $R_1$  and  $R_2$  are the inner and outer radii of the tube.

The polarizability of a single tube is obtained from the electric field induced by a quasi-static external field,  $E_{\text{ext}}$ . The component of the electric field parallel to the cylindrical axis is homogeneous. The perpendicular component of the electric field is  $E(\omega; r; \omega) = r \nabla V(\omega; r; \omega)$ . The electric field corresponding to a perpendicular external field  $E_{\text{ext}}$  is derived from the first Maxwell equation:

$$\nabla \cdot \epsilon_C(\omega; r; \omega) E(\omega; r; \omega) = 0; \quad (3)$$

with the boundary condition  $E(\omega; R_1; \omega) = E_{\text{ext}}$ . The electrostatic potential solution of Eq. (3) has the form:

$$V(\omega; r; \omega) = a_1 r \cos \theta; \quad (4)$$

$$V(\omega; r; \omega) = a_2 r^{(1)} + b_2 r^{(1)} \cos \theta; \quad (5)$$

$$V(\omega; r; \omega) = E_{\text{ext}} r + b_3 r^{-1} \cos \theta; \quad (6)$$

for  $r < R_1$ ,  $R_1 < r < R_2$  and  $r > R_2$ , respectively. Here  $\epsilon_C(\omega) = \epsilon_{zz}(\omega) = \epsilon_{rr}(\omega) = \epsilon_{\theta\theta}(\omega)$  and the scalar quantities  $a_1$ ,  $a_2$ ,  $b_2$  and  $b_3$  are determined by the continuity of  $V(\omega; r; \omega)$  and of the radial component of  $\epsilon_C(\omega; r; \omega) E(\omega; r; \omega)$  at the inner and outer surfaces of the tube. From these expressions, the transverse polarizability of the single tube  $\epsilon_p(\omega)$  can be derived (Eq. (4) of [1]). The macroscopic dielectric tensor of chrysotile,

$\epsilon_C(\omega)$ , is then obtained using an effective medium approach of Clausius-Mossotti type [4]:

$$\epsilon_{C,z}(\omega) = \epsilon^0 + (1 - f^0) \epsilon_p(\omega); \quad (7)$$

$$\epsilon_{C,p}(\omega) = 1 + \frac{f \epsilon_p(\omega)}{1 - f \epsilon_p(\omega) - 2}; \quad (8)$$

where  $\epsilon_{C,z}(\omega)$  and  $\epsilon_{C,p}(\omega)$  correspond to the components of  $\epsilon_C(\omega)$  parallel and perpendicular to the cylindrical axis, respectively,  $f$  is the volume fraction occupied by the tubes,  $f \approx 0.9$  for a close packed arrangement of the tubes and  $f^0 = f [1 - (R_1/R_2)^2]$ . From these equations, it can be shown that a single resonance in the dielectric tensor of the flat planar material,  $\epsilon_L(\omega)$ , can produce multiple resonances in  $\epsilon_p(\omega)$ , and therefore in the macroscopic dielectric constant  $\epsilon_{C,p}(\omega)$ . This behavior has been observed in Fig. 6 of Ref. [5]. The frequency for which confined plasmons occur, can be obtained as the non-zero solutions of Eqs. (4), (5) and (6) with  $E_{\text{ext}} = 0$ . In the limit of a vanishing damping coefficient, these resonances occur when  $D(\omega) = i(\omega)$  is real and satisfies:

$$D(\omega) \log(R_2/R_1) = 2 \tan^{-1} \epsilon_{\theta\theta}(\omega) D(\omega) + k; \quad (9)$$

where  $k$  is an integer. This equation admits an infinity of solutions because of the divergence of  $\epsilon_L(\omega)$  at a resonance with zero damping. In practice, the finite width of the resonances of  $\epsilon_L(\omega)$  leads to a finite number of resonances of  $\epsilon_C(\omega)$ , increasing with a decreasing ratio  $R_1/R_2$ .

To calculate the ATR spectra, we compute the reflection coefficient of an electromagnetic wave incident on a flat interface between the chrysotile medium, with dielectric tensor  $\epsilon_C(\omega)$ , and a Ge medium, with isotropic dielectric tensor equal to 16. The theoretical spectrum in absorbance unit is obtained as minus the logarithm of the reflection coefficient (Fig. 4). The main features and the changes of the spectra as a function of the polarization of the incident wave are very well reproduced by our calculations, with a ratio  $R_1/R_2 = 0.1$ , comparable with that observed by TEM (Fig. 2). The spectrum obtained with the electric field parallel to the  $c$  axis (Fig. 4, 1<sup>st</sup> panel) is described by  $\epsilon_{C,z}(\omega)$  and displays a single band ( $C_4$ , Tab. I). The spectra obtained with the electric field perpendicular to the  $c$  axis (Fig. 4, 2<sup>nd</sup> and 3<sup>rd</sup> panels) are described by  $\epsilon_{C,p}(\omega)$  and display three resonances ( $C_3$ ,  $C_2$ , and  $C_1$ , Tab. I). Finally, the spectrum obtained with the geometry of Fig. 4, last panel, contains resonances related to both  $\epsilon_{C,p}(\omega)$  and  $\epsilon_{C,z}(\omega)$ .

The theoretical powder IR transmission spectrum of chrysotile is computed using  $\epsilon_C(\omega)$  as in Ref. [15]. In this case, we consider that micrometric chrysotile particles are elongated along the  $z$  axis and inserted in a homogeneous KBr medium. An excellent agreement between the theoretical and the experimental spectrum is

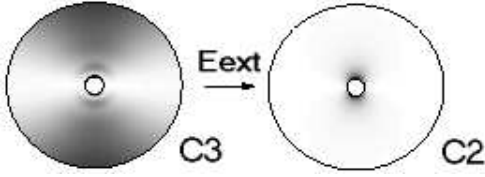


FIG. 5: Dissipated power density in the nanotube at the resonances  $C_2$  and  $C_3$ . The darker gray indicates larger dissipation. The arrow shows the direction of  $E_{\text{ext}}$ .

obtained (Fig. 3). In particular, the calculation reproduces the presence and the position of the strong absorption band at  $1018 \text{ cm}^{-1}$ , characteristic of chrysotile. By an analysis of the theoretical spectra, we can correlate the peaks observed in ATR to those observed in transmission. In particular, we find that the peaks at  $1084$  and  $1018 \text{ cm}^{-1}$  in transmission are associated to the resonances  $C_1$  and  $C_2$ , whereas the resonance at  $961 \text{ cm}^{-1}$  is mainly associated to  $C_4$ , and in a minor proportion to  $C_3$ . The frequency shifts and intensity changes of the bands between the ATR and the transmission spectra arise from the different geometry of the two experimental setups, and are reproduced by our calculations.

Our theoretical investigation of the IR spectrum of chrysotile also provides an unambiguous assignment of the resonances with respect to the vibrational modes of the layers, Tab. I. The out-of-plane Si-O stretching mode leads to  $C_1$ . The in-plane Si-O stretching mode polarized parallel to the cylindrical axis of the tube leads to  $C_4$ . The other in-plane Si-O stretching mode, perpendicular to the cylindrical axis, leads to the two resonances  $C_2$  and  $C_3$ , that correspond to the solutions of Eq. (9) for  $k=1$  and  $k=2$ , respectively. Therefore, the resonances  $C_2$  and  $C_3$  are related to two distinct localized plasmons which originate from the same resonance in the dielectric tensor of lizardite. We study the spatial extension of these two plasmons by looking at the spatial distribution of the dissipated power density,  $W(r; \omega)$  [15]. In Fig. 5, we report  $W(r; \omega)$  for an isolated tube for the resonances  $C_2$  and  $C_3$ . The resonance  $C_2$  is related to a surface plasmon localized at the internal surface of the nanotube. The resonance  $C_3$  is distributed over the whole tube, and presents two nodes close to the inner surface (Fig. 5). Note that, in our calculations, the two in-plane Si-O stretching modes of the layered local crystal structure are still degenerate. Therefore, the splitting of the Si-O stretching absorptions bands in the IR spectra of chrysotile is not related to a change in the microscopic structure of the layer induced by the bending of the tetrahedral sheets, as previously proposed [10].

In conclusion we have shown, by experiment and theory, that multiple plasmons are observed in the IR spectra of chrysotile nanotubes. In particular a single in plane Si-O stretching mode of the  $\text{Mg}_3\text{Si}_2\text{O}_5(\text{OH})_4$  layer produces two resonances in the polarisability of chrysotile.

TABLE I: Theoretical transverse optical (TO) modes and corresponding resonances of the IR spectra. Experimental values in parenthesis. With jj and ? we indicate the Si-O modes parallel and perpendicular to the  $\text{Mg}_3\text{Si}_2\text{O}_5(\text{OH})_4$  layers, and with  $u_r$ ,  $u_\phi$ , and  $u_z$ , the dominant cylindrical polarization.

	polarization	TO	label	transmission	ATR
Lizardite	jj	1045	$L_1$	1105 (1084)	–
	?	951	$L_2$	951 (951)	–
Chrysotile	jj $u_r$	1045	$C_1$	1077 (1084)	1071 (1075)
	? $u_\phi$	951	$C_2$	1022 (1018)	992 (995)
	? $u_\phi$	951	$C_3$	972	955 (955)
	? $u_z$	951	$C_4$	951 (961)	936 (938)

We have predicted that the number of resonances increases with a decreasing width of the vibrational modes and/or a decreasing ratio between the inner and outer radii of the nanotubes. Thus we anticipate that more resonances should be detected in chrysotile samples or other nanotube systems which optimize these parameters. Finally the IR plasmons resonances could become a tool to monitor the geometrical parameters of nanotube based materials.

Calculations were performed at the IDRIS, and TEM work at the French INSU National Facility, CRM C2-CNR S, Marseille. This is IGP contribution # 0000.

- 
- [1] L. Henrard and P. Lambin, J. Phys. B 29, 5127 (1996).
  - [2] W. de Heer, W. Bacsá, A. Châtelain, T. Ger n, R. Hum phrey-Baker, L. Forro, and D. Ugarte, Science 268, 845 (1995).
  - [3] F. Garcia-V idal and J. Pendry, Phys. Rev. Lett. 77, 1163 (1996).
  - [4] F. Garcia-V idal, J. Pitarke, and J. Pendry, Phys. Rev. Lett. 78, 4289 (1997).
  - [5] M. Kociak, L. Henrard, O. Stephan, K. Suenaga, and C. Colliex, Phys. Rev. B 61, 13936 (2000).
  - [6] M. Kociak, O. Stephan, L. Henrard, V. Charbois, A. Rothschild, R. Tenne, and C. Colliex, Phys. Rev. Lett. 87, 075501 (2001).
  - [7] F. Wicks and D. O'Hanley, in Hydrous phyllosilicates (exclusive of mica), edited by S. Bailey (Miner. Soc. Amer., Washington, 1988), vol. 19 of Reviews in Mineralogy, pp. 91-167.
  - [8] C. Vitelli and M. Mellini, Euro. J. Miner. 9, 585 (1997).
  - [9] V. Famer, The infrared spectra of minerals (Mineralogical Society, London, 1974).
  - [10] S. Yaviv and L. Heller-Kallai, Clays Clay Miner. 23, 145 (1975).
  - [11] C. Lemaire, F. Guyot, and B. Reynard, unpublished.
  - [12] M. Titulaer, J. C. van Miltenburg, H. Ben, J. Jansen, and J. Geus, Clays Clay Miner. 41, 496 (1993).
  - [13] E. Balan, A. Saitta, F. Mauri, C. Lemaire, and F. Guyot, Amer. Miner. (2002), in press.
  - [14] S. Baroni, S. de Gironcoli, A. D. Corso, and P. Giannozzi, Rev. Mod. Phys. 73, 515 (2001).

- [15] E . Balan, A . Saitta, F . M auri, and G . Calas, Amer. Miner. 86, 1321 (2001).